metals

MDPI

Article

Recovery of Vanadium (V) Oxyanions by a Magnetic Macroporous Copolymer Nanocomposite Sorbent

Ljiljana Suručić [1], Tamara Tadić [2], Goran Janjić [2], Bojana Marković [2], Aleksandra Nastasović [2] and Antonije Onjia [3,*]

[1] Faculty of Medicine, University of Banja Luka, Save Mrkalja 14, 78000 Banja Luka, Bosnia and Herzegovina; ljiljana.surucic@med.unibl.org
[2] Institute of Chemistry, Technology and Metallurgy, University of Belgrade, Njegoševa 12, 11000 Belgrade, Serbia; tamara.tadic@ihtm.bg.ac.rs (T.T.); goran_janjichem@yahoo.com (G.J.); ekmescicbojana@gmail.com (B.M.); aleksandra.nastasovic@ihtm.bg.ac.rs (A.N.)
[3] Faculty of Technology and Metallurgy, University of Belgrade, Karnegijeva 4, 11000 Belgrade, Serbia
* Correspondence: onjia@tmf.bg.ac.rs

Abstract: An amino-functionalized magnetic macroporous copolymer of glycidyl methacrylate (GM) and ethylene glycol (E) dimethacrylate (m-poly(GME)-deta) was synthesized, fully characterized, and used to investigate the adsorption of vanadium (V) oxyanions from aqueous solutions (Ci = 0.5 mM) in a batch system at room temperature (298 K). Pseudo-first-order (PFO), pseudo-second-order (PSO), Elovich, and intra-particle diffusion (IPD) models were used to analyze the kinetic data. The study showed that sorption is rapid, i.e., the sorption half-time is approximately one minute. Initially, the sorption process primarily involved surface sorbent particles, and it was best described by the PSO model. However, after saturation of the surface active sites is attained, the sorption rate decreases significantly because of limitations of the diffusion rate, which is then primarily controlled by the IPD process. The sorption process is favorable in the pH range of 3–6 due to the strong electrostatic interactions between the absorption centers of copolymer and vanadium (V) oxyanions. In the stated pH range, deta absorption centers with two and three protonated N atoms are in equilibrium as studied by quantum chemical modeling. Among V(V) species present in diluted aqueous media, the adsorption of $H_2VO_4^-$ ions dominates.

Keywords: glycidyl methacrylate; quantum chemical modeling; Eh–pH; silanization; adsorption; vanadate

Citation: Suručić, L.; Tadić, T.; Janjić, G.; Marković, B.; Nastasović, A.; Onjia, A. Recovery of Vanadium (V) Oxyanions by a Magnetic Macroporous Copolymer Nanocomposite Sorbent. *Metals* **2021**, *11*, 1777. https://doi.org/10.3390/met11111777

Academic Editor: Manuel Aureliano

Received: 19 October 2021
Accepted: 2 November 2021
Published: 4 November 2021

1. Introduction

Vanadium occurs in nature in the form of 65 different minerals, mostly vanadinite, descloisite, carnotite, and patronite. Natural sources of vanadium in the atmosphere include dust (crushed soil particles), marine aerosol and volcanic emissions, anthropogenic industrial products, and fossil fuel byproducts. Sorption of vanadium (V) from aqua solution onto natural soil colloids depends on pH and ionic strength conditions [1]. Vanadium is widely used as a steel additive and catalyst in the metallurgical and chemical industries [2], and while being found in traces in nature, it represents a significant raw material. Various processes for the extraction of vanadium from the complex metallic mixture are in usage nowadays [3–6], but only a few are environmentally friendly.

Several studies showed that amino-functionalized GM-based copolymers possess a significant affinity for the sorption metal ions [7,8]. Moreover, these polymers are characterized by thermal and chemical stability [9,10]. Embedding magnetic particles in the polymer matrix of GMA further extends their functionality, simplifying the removal process by applying a magnetic field [11,12]. It was shown that the metal ion sorption process on the surface of macroporous polymer nanocomposites depends on various parameters, such as the properties of the sorbent (chemical structure, porosity, specific surface area, particle

size), ion properties (chemical nature and charge), and sorption conditions, such as ion concentrations in solution, pH, temperature, presence of other competing species, and contact time. In this study, an amino-functionalized magnetic macroporous copolymer of GM and E dimethacrylate synthesized by in situ suspension copolymerization in the presence of Fe_3O_4 (m) nanoparticles coated with 3-aminopropyltrimethoxysilane (APTMS) through a silanization process, functionalized with diethylene triamine (deta), m-Si-poly(GME)-deta, was fully characterized in terms of its structural properties and tested as a sorbent of vanadium (V) oxyanions.

2. Materials and Methods

The tested sorbent m-Si-poly(GME)-deta was synthesized as described in previous works [13]. Pore size distributions were determined by a high-pressure mercury intrusion porosimeter Carlo Erba Porosimeter 2000 (Washington, DC, USA, software Milestone 200). The SEM/EDX analysis of sorbent was performed on a JEOL JSM-6610LV SEM instrument (JEOL Inc., Peabody, MA, USA) equipped with EDX detector (X-Max Large Area Analytical Silicon Drift connected with INCA Energy 350 Microanalysis System, Oxford Instruments Nanoanalysis, High Wycombe, UK) after sputtering with gold in order to enable the imaging and to prevent thermal damage of the specimen.

The thermogravimetric analysis (TGA) (30–700 °C range) was performed on SDT Q600 TGA/DSC instrument (TA Instruments, New Castle, DE, USA). Heating rates were 20 °C/min using less than 10 mg sample mass. The furnace atmosphere consisted of dry nitrogen at a flow rate of 100 cm^3/min. Further, m-Si-poly(GME)-deta was used to investigate the sorption of vanadium (V) oxyanions from diluted aqueous solutions (C_0 = 25 ppm) in a batch system at room temperature (298 K). The oxyanion concentrations in a solution were determined by inductively coupled plasma optical emission spectrometry (ICP-OES) (model Thermo Scientific iCAP 6500, Waltham, MA, USA). The PFO, PSO, Elovich, and IPD models were used to analyze the kinetic data.

A freshly prepared solution of ammonium metavanadate NH_4VO_3 p.a. purity (Acros Organic, Belgium) in deionized water (Milli-Q Millipore, conductivity 18 MΩ/cm) was used for the sorption assay.

The sorption capacity, i.e., the amount of vanadium (V) sorbed onto a unit mass of magnetic sorbent, Q, was calculated from:

$$Q = \frac{(C_i - C) \times V}{m} \quad (1)$$

where C_i and C are initial and concentration in the sample after sorption, V is the solution volume, and m is the sorbent mass.

Kinetic data were analyzed with the PFO (Equation (2)), PSO (Equation (3)), Elovich (Equation (4)), and IPD (Equation (5)):

$$\frac{dQ_t}{dt} = k_1 \times (Q_e - Q_t) \quad (2)$$

$$\frac{dQ_t}{dt} = k_2 \times (Q_e - Q_t) \quad (3)$$

where Q_e (mg/g) and Q_t (mg/g) are the amounts of sorbed ions at equilibrium and at time t,

$$\frac{dQ_t}{dt} a_e \times e^{-b_e Q_t} \quad (4)$$

where a_e is initial sorption rate (mg/g·min or mmol/g·min) and b_e is a parameter determined by the surface coverage that depends on the activation energy during chemisorption (g/mg or g/mmol) [14]:

$$Q_t = k_{id} t^{0.5} \quad (5)$$

where Q_e (mg/g) and Q_t (mg/g) are the amounts of sorbed ions at equilibrium and at time t, respectively, $\alpha_e = Q_t/Qe$ is fractional attainment of equilibrium, K_p is the film diffusion rate constant, D_F is a parameter of the linear driving force, k_{id} is the intraparticle diffusion coefficient (μmol/g·min$^{0.5}$), t is the time, and C_{id} is a constant, related to the thickness of the boundary layer.

For equilibrium data analysis, the Langmuir (Equation (6)), Freundlich (Equation (7)), and Tempkin (Equation (8)) isotherm models were used [15]:

$$\frac{C_e}{Q_e} = \frac{1}{Q_{max}K_L} + \frac{C_e}{Q_{max}} \quad (6)$$

$$lnQ_e = lnK_F + \frac{1}{n}lnC_e \quad (7)$$

$$Q_e = \frac{RT}{b}lnK_T + \frac{RT}{b}lnC_e \quad (8)$$

where Q_{max} (mg/g) is the Langmuir maximum adsorption capacity, K_L (L/mg) is the Langmuir isotherm constant, K_F (mg/g)(g/L)$^{1/n}$ and n are the Freundlich constant and isotherm exponent, respectively, K_T (L/mg) is the Tempkin isotherm equilibrium binding constant, b_T (mg/L) is the Tempkin isotherm constant, R is the gas constant (8.314 J/mol K), and T is the absolute temperature (K).

The efficiency of the adsorption process can be predicted by the dimensionless Langmuir equilibrium parameter R_L:

$$R_L = \frac{1}{1 + K_L C_0} \quad (9)$$

The value of R_L indicates the type of the isotherm either to be unfavorable ($R_L > 1$), linear ($R_L = 1$), favorable ($0 < R_L < 1$) or irreversible ($R_L = 0$).

The quantum chemical calculations were performed using the Gaussian09 software package. (Gaussian, Inc.). Four possible dimers of the studied systems were optimized by using the B3LYP functional, 6-311+g** basis set for non-metals, lanl2dz basis set for vanadium, and solvation model based on density (SMD) for water solvent. At the same level of theory, the interaction energies between vanadium (V) oxyanions and detaOH absorbent in the optimized dimer structures were calculated. DetaOH represents the chemical species formed in the reaction of deta amine and 1,2-epoxyethane, used as a model for the adsorption centers in the copolymer.

3. Results

3.1. Structural Characterization

The porosity parameters for sample m-Si-poly(GME)-deta, i.e., the values of specific pore volume, V_s, and pore diameter corresponding to half of pore volume, $D_{V/2}$, were read from the pore size distribution curves determined by mercury porosimetry, while the specific surface area, $S_{s,Hg}$, was calculated as the sum of incremental specific surface areas from the pore size distribution curves as described in the literature [16]. Calculated values are presented in Table 1, along with the data for different samples of the macroporous copolymer of glycidyl methacrylate and ethylene glycol dimethacrylate: magnetic non-functionalized specimen m-poly(GME), magnetic sample grafted with diethylene triamine m-poly(GME)-deta, obtained in literature [17], and magnetic silanized non-functionalized m-Si-poly(GME).

Table 1. Porosity parameters of investigated samples.

Sample	V_s, cm^3/g	$S_{s,Hg}$, m^2/g	$D_{V/2}$, nm
m-poly(GME) *	1.08	67	100
m-Si-poly(GME)	1.32	32	272
m-poly(GME)-deta *	0.99	59	104
m-Si-poly(GME)-deta	1.20	37	286

* Literature data modified from [17].

The silanization of magnetite leads to the sample with 2.7 times larger pore diameter and an almost 50% reduction in $S_{s,Hg}$ values compared to the non-silanized sample ($D_{V/2}$ = 100 nm and $S_{s,Hg}$ = 67 m^2/g for m-poly(GME) [17]). As illustrated in Table 1, amino-functionalization had no influence on porosity parameters.

Characterization of the m-Si-poly(GME)-deta sorbent by SEM microscopy (Figure 1) clearly indicated the presence of spherical particles, very smooth and uniform in morphology.

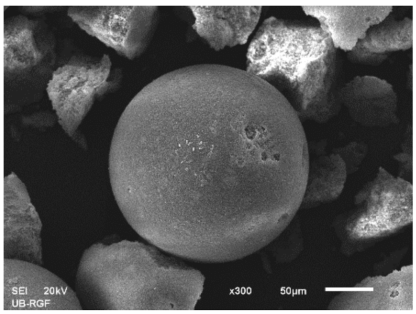

Figure 1. SEM micrographs of m-Si-poly(GME)-deta particles.

As expected, the most intense peaks in the EDX spectrum (Figure 2) originate from elements C and O. The presence of Fe peaks clearly indicates the incorporation of magnetite. A stronger Fe peak was detected on the surface of the sample particles and the Si peak (which confirms the silanization of magnetite particles). The N peak indicates the functionalization of amino groups and is predominantly oriented on the inner surface of the particles (~14 w/w % at the cross-section and 4.7 w/w % at the particle surface). The peak for Au in the SEM/EDX spectrum originates from Au coating of the m-Si-poly(GME)-deta.

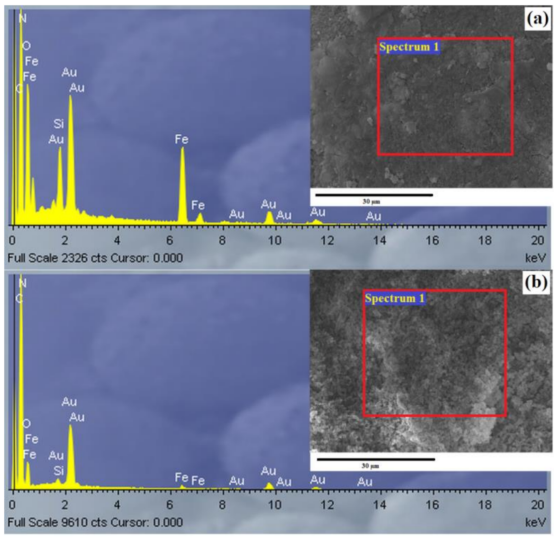

Figure 2. SEM-EDX spectrum of particle surface (**a**) and cross section (**b**) of m-Si-poly(GME)-deta (scale bar: 30 µm).

As one can see, TGA thermograms for both samples exhibited a multiple-step degradation pattern. The primary degradation mechanism of the samples is depolymerization to monomers and oligomers initiated by scission of weak linkages (i.e., H-H bonds, double bonds in backbone pendant groups and random chain scission) and ester decomposition that simultaneously occur [18]. Besides depolymerization and ester decomposition, the thermal degradation of m-Si-poly(GME)-deta also involves the elimination of amine groups. In addition, an initial loss of about 6 wt. % below 100 °C might be assigned to the loss of physically retained or occluded solvents [19,20]. The weight loss in the temperature range of 30–190 °C was mainly from the elimination of molecular water adsorbed on the copolymer surface.

The TGA curves were presented in Figure 3. The main parameters evaluated on the basis of these curves are presented in Table 2.

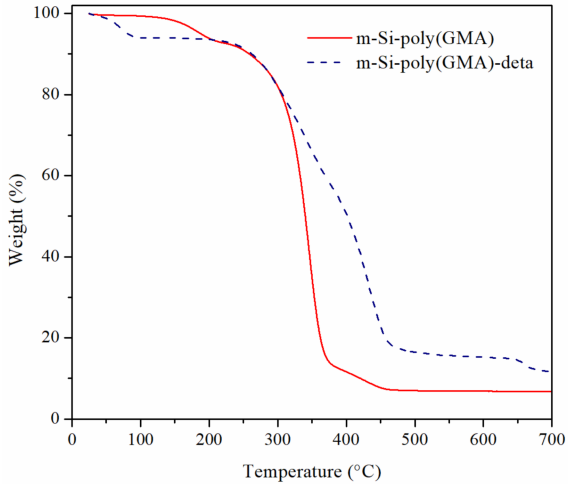

Figure 3. TGA curves of m-Si-poly(GME) and m-Si-poly(GME)-deta.

Table 2. The results of TGA for investigated samples.

Sample	Degradation Steps, T (°C)			T_{max} (°C)	$T_{5\%}$ (°C)	$T_{10\%}$ (°C)	$T_{50\%}$ (°C)
	I	II	III				
m-Si-poly(GME)	30–220	220–400	400–470	182/347/430	187	260	342
m-Si-poly(GME)-deta	30–100	100–370	370–560	70/342/430	83	260	400

Since the boiling point of APTMS is 194 °C, physically adsorbed APTMS is completely desorbed to 300 °C [21]. The main decomposition of chemically bonded APTMS occurred up to 470 °C and 560 °C for m-Si-poly(GME) and m-Si-poly(GME)-deta, respectively. This is in agreement with the literature data showing that the thermal decomposition of grafted silane takes place at above 450 °C and the breaking of the C–Si bond starts at 450–510 °C [21,22].

A significant loss in both samples was observed during the second degradation step. The residue values (7 and 11 wt % for m-Si-poly(GME) and m-Si-poly(GME)-deta, respectively) are in agreement with the magnetite content incorporated in the investigated samples.

3.2. Vanadium Sorption

In this study, the sorption capacity of m-Si-poly(GME)-deta in diluted vanadium solution (0.5 mM) as a function of concentration, contact time, and pH was tested.

The experimental isotherm data are shown in Figure 4.

Sorption was rapid. The sorption half time, $t_{1/2}$ (the time required to reach 50% of the total sorption capacity) was approximately 1 min and the sorbent saturation Q_{max} was achieved after 120 min. The maximum sorption capacity was 28.7 μmol/g.

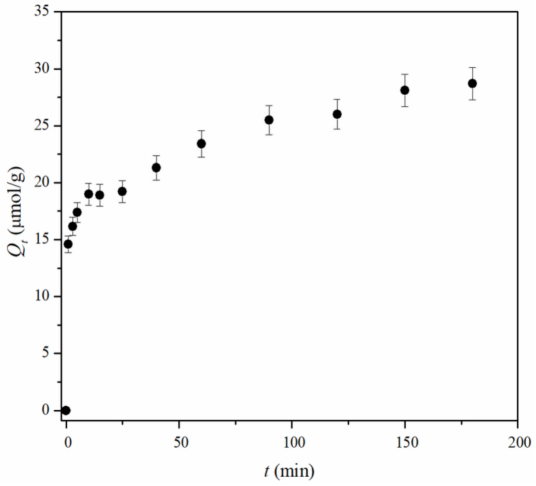

Figure 4. Effect of contact time on V(V) sorption from aqueous solutions onto m-Si-poly(GME)-deta (pH = 5.0, initial ions concentration: 25 mg/dm^3 and T = 298 K).

4. Discussion

4.1. Effect of pH

Vanadium speciation in an aqueous system is a complex function of concentration, pH, redox potential (oxidation/reduction potential, i.e., E_h), and solution chemistry (Figure 5). Vanadium exists in the +3, +4, and +5 oxidation states in natural waters. Vanadate species [V(V)] are thermodynamically stable in oxic conditions, while V(IV) is stable under suboxic conditions, and V(III) is found in anoxic environments [23].

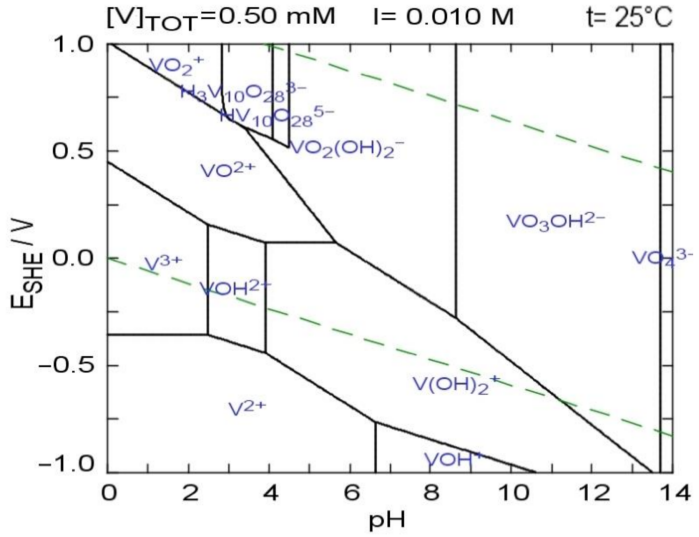

Figure 5. Pourbaix (Eh–pH) diagram for vanadium (V) species. Dashed lines represent the upper (oxygen generation) and the lower (hydrogen formation) stability limits of water.

Figure 6 shows that the speciation of vanadium is a strong function of concentration and pH. At the low vanadium concentrations, the following V(V) species are dominantly present in the solution: the pervanadyl ion, VO^{2+}, vanadic acid, $H_3VO_4{}^0$, and its three conjugate bases, H_2VO^{4-}, $HVO_4{}^{2-}$, and $VO_4{}^{3-}$.

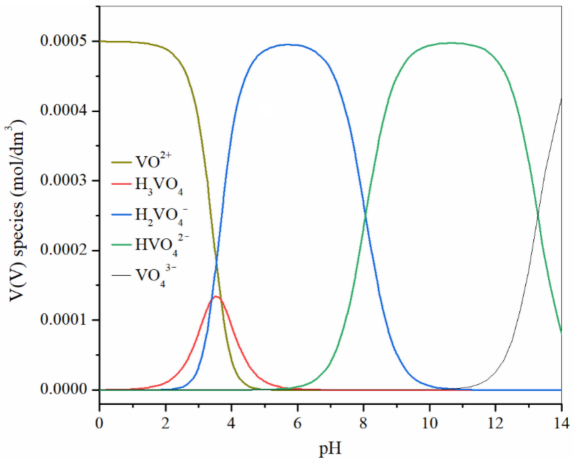

Figure 6. Distribution of vanadium (V) species as a function of pH (Ionic strength: 0.01 M; total vanadium concentration: 0.5 mM).

In dilute solutions at neutral pH, the dominant species of V(V) are the phosphate-like mononuclear vanadate oxyanions $H_nVO_4^{n-3}$. The species VO^{2+} dominates under acidic conditions, and VO_4^{3-} occurs in extremely alkaline conditions. Vanadic acid, $H_3VO_4^0$, is a minor constituent within the narrow pH range 3–4. Vanadium has a notable tendency to oligomerize, forming species containing up to 10 atoms of V [23]. The mass action, charge, and mass balance equations [24] used to generate Figures 5–7 were solved using the computer program written in Mathcad by one of the authors (A.O.). Relevant thermodynamic data were taken from literature [25].

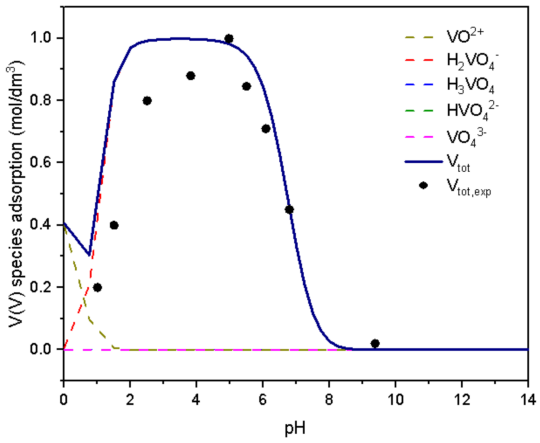

Figure 7. Effect of pH on V(V) sorption from aqueous solutions onto m-Si-poly(GME)-det. Blue, green and magenta dashed lines represent all zero values.

The sorption process of V(V) ions is dependent on pH of the equilibrium solution. The influence of pH on the adsorption of V(V) was investigated in the pH range of 2.5–11.0 with a contact time of 60 min and V(V) concentration fixed at 0.5 mM in a batch system, at room temperature (298 K). The results are shown in Figure 7. It was observed that the adsorption percentage of V(V) was significantly high in the aqueous solution pH range from 3.0 to 6.0, and maximum adsorption for the V(V) was obtained at pH 5.0. When the pH was further increased from 6.0 to 8.0, the adsorption percentage decreased.

When the pH of the solution is higher than 6.0, the decreased adsorption efficiency of V(V) ions might result from the other V(V) oxidation states that form at high pH, such as $V_3O_9^{3-}$, HVO_4^{2-}, and $HV_2O_7^{3-}$, and which might affect the adsorption capacity on the m-Si-poly(GME)-deta. Thus, pH 5.0 was adopted for further studies. Similar behavior has

been reported for V(V) adsorption on chitosan-zirconium (IV) [26], biomass [27], and other oxyanions on similar sorbents [17,28–31].

4.2. Sorption Isotherms

The experimental isotherm data (Figure 8a) have been fitted with Langmuir, Freundlich, and Tempkin equations (Figure 8b–d).

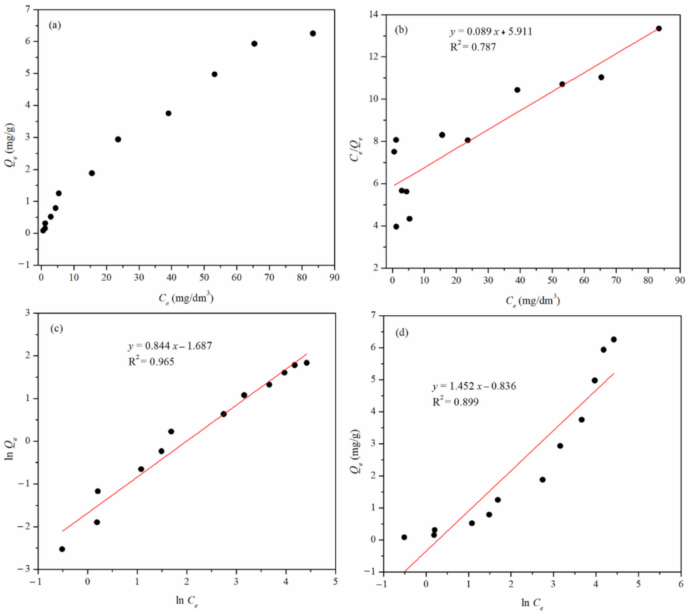

Figure 8. Adsorption isotherm of V(V) sorption onto m-Si-poly(GME)-deta (T = 298 K, t = 60 min, P = atm) (**a**), Langmuir (**b**), Freundlich (**c**) and Tempkin (**d**) isotherms.

Isotherm parameters and regression data are presented in Table 3.

Table 3. Isotherm parameters and regression data for V(V) sorption on m-Si-poly(GME)-deta at 298 K.

Isotherm Models	Parameters	V(V)
Langmuir	Q_{max} (mg/g)	11.23
	K_L (1/mg·dm)	0.015
	R_L	0.0067
	R^2	0.79
Freundlich	n_f	1.18
	K_F (mg/g)(mg/L)$^{1/n}$	0.18
	R^2	0.96
Tempkin	A_T (dm^3/mg)	0.56
	b_T (kJ/mg)	1.71
	R^2	0.90

Sorption capacity increases with higher initial concentration. Freundlich isotherms could be identified as the most suitable for modeling the equilibrium sorption behavior and the process could be described as multilayer sorption of the presence a number of vacant active sites. Besides, as the value of the parameter was calculated as n_f = 1.18, it is indicative of a chemisorption process [32]. The values of the Freundlich constants and R_L value suggest that the sorption process of oxyanion V(V) is favored by the magnetic sorbent m-Si-poly(GME)-deta.

4.3. Kinetic Models of Sorption

Sorption kinetic data were analyzed using the surface-reaction (PFO and PSO), Elovich, and particle diffusion-based (IPD) kinetic models to investigate the controlling mechanism of V(V) sorption by m-Si-poly(GME)-deta (Figure 9). Kinetic parameters calculated from these models are presented in Table 4, where Q_t denotes the amount of sorbed metal ions at time t, Q_e the amount of sorbed metal ions at equilibrium, k_1 the PFO rate constant, k_2 the PSO rate constant, b_e the Elovich parameter determined by the surface coverage, k_{id} the IPD coefficient, and C_{id} the intercept of the IPD plot.

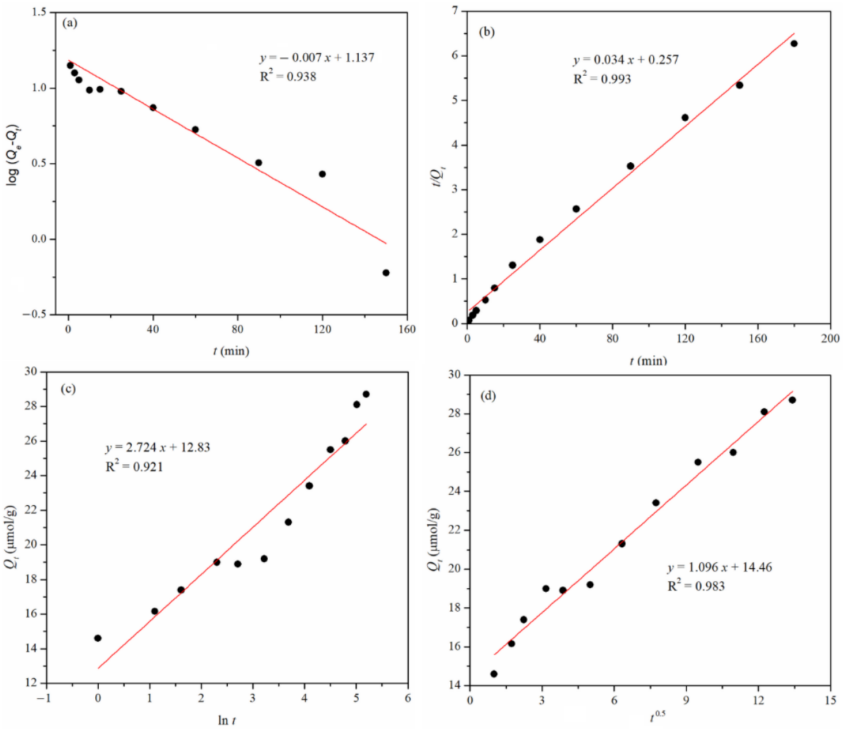

Figure 9. (**a**) PFO, (**b**) PSO, (**c**) Elovich and (**d**) IPD kinetic plots for V(V) sorption on solutions onto m-Si-poly(GME)-deta.

Table 4. PFO, PSO, Elovich and IPD kinetic parameters V(V) ion sorption using m-Si-poly(GME)-deta.

PFO			
k_1 1/min	Q_e μmol/g		R^2
0.016	13.7		0.938
PSO			
k_2 g/(μmol·min)	Qe μmol/g	h μmol/(g·min)	R^2
0.0045	29.41	3.89	0.993
Elovich			
a_e μmol/(g·min)	b_e g/μmol		R^2
302.5	0.37		0.921
IPD			
k_{id} (μmol/g)·min$^{-0..5}$	C_{id} μmol/g		R^2
1.10	14.5		0.983

The sorption of oxyanions on m-Si-PGME-deta is initially very fast. The sorption half time, $t_{1/2}$ (the time required to reach 50% of the total sorption capacity), was approximately $t_{1/2} < 2$ min and the sorbent saturation Q_{max} is achieved after 40 min. The PSO model is applicable only during the initial stage when the sorption process is film diffusion-controlled because oxyanions are bound on the surface of the sorbent particles. As the saturation rate of active surface sites gradually increases, the process becomes interparticle-diffusion controlled and data are better described by the IPD model.

4.4. Quantum Chemical Modeling

To understand the absorption profile of copolymer as a function of pH value, quantum-chemical calculations were performed on several model systems. Model systems contain two chemical species. The first species is an absorbent (detaOH absorption center of the copolymer, Figure 10) while the second one is vanadium (V) oxyanion. Absorption is monitored in the pH region from 2 to 9, in which the three absorption centers (detaOH-H_3^{3+}, detaOH-H_2^{2+}, and detaOH-H^+) are in equilibrium [33].

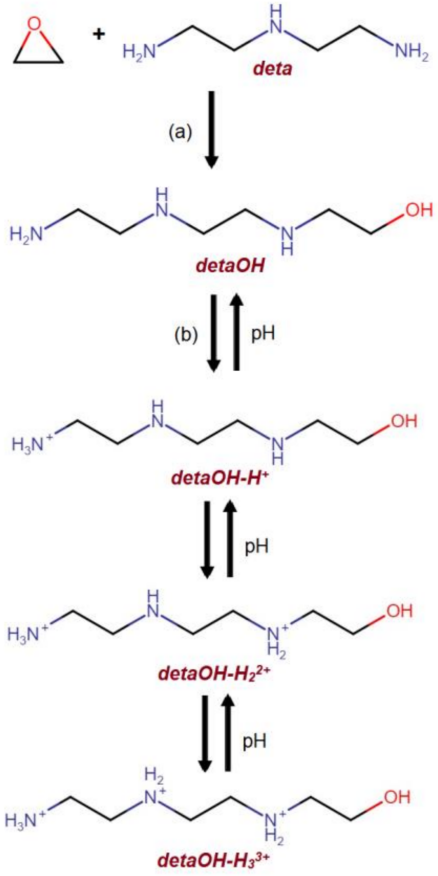

Figure 10. The reaction of functionalization of starting epoxy copolymer by deta amine (**a**) and the equilibrium of detaOH absorption centers (**b**) used in model systems for estimation of the binding energies of vanadium (V) oxyanion to the copolymer.

Vanadium (V) oxyanions are attracted by electrostatic forces of copolymer, which are reinforced by N-H $\cdots$ O, O-H $\cdots$ N, and C-H $\cdots$ O hydrogen bonds (Figure 11). However, the VO_2^+ cation is the most common vanadium (V) species in solution with pH $\leq$ 3 (Figure 5), the absorption of vanadium species originates from the vanadic acid (H_3VO_4), which is present in appreciable quantities. H_3VO_4 interacts with the detaOH-H_3^{3+} absorption center with an interaction energy of -55.9 kcal/mol (Table 5). The interaction between VO^{2+} ion and detaOH-H_3^{3+} would be repulsive due to the same charge of both species.

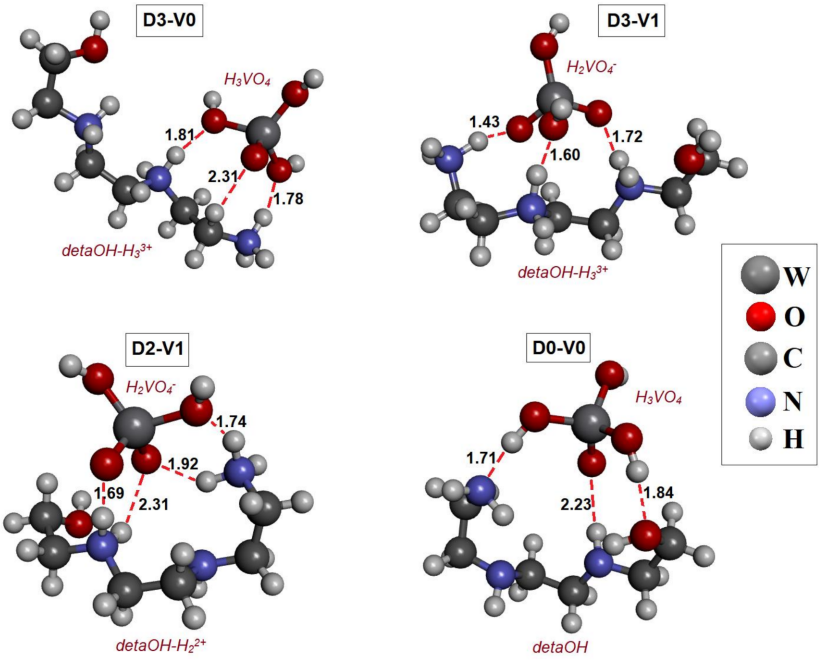

Figure 11. The optimized structures of dimers (bond lengths are given in Å), used to estimate the interaction energies between vanadium (V) oxyanions and detaOH absorbent. D3, D2, D0, V0 and V1 abbreviations in the labels of dimers refer to detaOH-H_3^{3+}, detaOH-H_2^{2+}, detaOH, H_3VO_4, and $H_2VO_4^-$, respectively.

Table 5. The labeling of starting and optimized dimers and calculated energies of interactions (in kcal/mol) between vanadium (V) oxyanions and detaOH absorbent.

Starting Geometry	Optimized Geometry	Abbreviation of Dimer	Interaction Energy
detaOH-$H_3^{3+}\cdots H_3VO_4$	detaOH-$H_3^{3+}\cdots H_3VO_4$	D3-V0	−55.9
detaOH-$H_3^{3+}\cdots H_2VO_4^-$	detaOH-$H_3^{3+}\cdots H_2VO_4^-$	D3-V1	−311.6
detaOH-$H_2^{2+}\cdots H_2VO_4^-$	detaOH-$H_2^{2+}\cdots H_2VO_4^-$	D2-V1	−203.4
detaOH-$H_2^{2+}\cdots HVO_4^{2-}$	detaOH$\cdots H_3VO_4$	D0-V0	−44.8

In the pH range from 3 to 8, the negatively charged $H_2VO_4^-$ ion becomes the most abundant vanadium (V) oxyanion in the solution. Due to their opposite charges, $H_2VO_4^-$ ion builds much stronger interactions with detaOH-H_3^{3+} center (−311.6 kcal/mol) than H_3VO_4 (−55.9 kcal/mol). The second detaOH absorption center (detaOH-H_2^{2+}) occurs at pH greater than 2, and it is the main absorption center in the pH range from 5 to 9. Due to the less positive charge, detaOH-H_2^{2+} builds weaker interactions with $H_2VO_4^-$ ion (−203.4 kcal/mol) than detaOH-H_3^{3+} center (−311.6 kcal/mol).

According to calculations, it should be expected that the absorption increases up to pH = 5, and after that, it should decline. As the detaOH-H_2^{2+} and detaOH-H_3^{3+} species are in equilibrium up to pH = 6.5 (when the detaOH-H_3^{3+} species disappears), the increase in absorption up to pH = 6 is understandable when the maximum of absorption is monitored. As detaOH-H_2^{2+} completely replaces detaOH-H_3^{3+} species in solution at pH greater than 7, a decrease in absorption is expected.

In order to complete the absorption profile of copolymer, another ionic species of vanadium (V) should be considered. Namely, the HVO_4^{2-} ion appears at pH = 7 (Figure 10), which has a higher negative charge than the $H_2VO_4^-$ ion. This should result in an increase of absorption due to greater electrostatic attraction in detaOH-$H_2^{2+}\cdots HVO_4^{2-}$ system than in detaOH-$H_2^{2+}\cdots H_2VO_4^-$ system. However, the optimization of the detaOH-$H_2^{2+}\cdots HVO_4^{2-}$ system is accompanied by the transition of two H ions from the detaOH-H_2^{2+} to HVO_4^{2-} species, resulting in the formation of a system with two neutral species

(detaOH $\cdots$ H_3VO_4 system) (Figure 11). Therefore, the interaction energy is significantly lower (−44.8 kcal/mol) than the interaction energy in detaOH-H_2^{2+} $\cdots$ $H_2VO_4^-$ system (−203.4 kcal/mol). The transition of H ions could explain the decrease in adsorption at pH values greater than 7.

The appearance of detaOH- H^+ species at pH greater than 7 (Figure 10) also contributes to a decrease in absorption. However, this contribution is probably negligible due to the equilibrium of detaOH-H_2^{2+} and detaOH-H^+ species.

5. Conclusions

Two different macroporous glycidyl methacrylate and ethylene glycol dimethacrylate copolymer sorbents were synthesized: magnetic silanized non-functionalized and magnetic silanized grafted with diethylene triamine (deta). The sorbent particles are spherical as well as chemically and thermally stable. Pore size and surface functionalization were efficiently controlled during the synthesis. The sorption kinetics for V(V) oxyanions adhered to the PSO model, implying an important role of chemisorption in the sorption process, with the evident influence of the intraparticle diffusion. Major V(V) species that are adsorbed from the diluted aqueous solution are $H_2VO_4^-$ ions. The process is favorable at the acidic pH values, while the adsorption in alkaline solution is negligible. In acidic solutions, the electrostatic interactions between the absorption centers of copolymer and vanadium (V) oxyanions are the strongest. The absorption centers in this medium have the highest possible positive charge (+3 and +2), located on N atoms of the deta group. The increase of pH value leads to a reduction in the positive charge of the surface adsorption centers, thereby reducing the driving (electrostatic) force between the copolymer and oxyanions.

Author Contributions: Conceptualization, A.O.; methodology, A.N.; validation, T.T.; formal analysis, G.J.; data curation, G.J.; writing—original draft preparation, L.S.; writing—review & editing, A.O. visualization, B.M. and A.N.; supervision, A.N. All authors have read and agreed to the published version of the manuscript.

Funding: This work was financially supported by the Ministry of Education, Science and Technological Development of the Republic of Serbia (Grant No. 451-03-9/2021-14/200026 and 451-03-9/2021-14/200135).

Data Availability Statement: Data presented in this article are available at request from the corresponding author.

Conflicts of Interest: The authors declare no conflict of interest.

References

1. Luo, X.; Yu, L.; Wang, C.; Yin, X.; Mosa, A.; Lv, J.; Sun, H. Sorption of vanadium (V) onto natural soil colloids under various solution pH and ionic strength conditions. *Chemosphere* **2017**, *169*, 609–617. [CrossRef]
2. Ma, Y.; Wang, X.; Stopic, S.; Wang, M.; Kremer, D.; Wotruba, H.; Friedrich, B. Preparation of Vanadium Oxides from a Vanadium (IV) Strip Liquor Extracted from Vanadium-Bearing Shale Using an Eco-Friendly Method. *Metals* **2018**, *8*, 994. [CrossRef]
3. Li, X.; Wei, C.; Deng, Z.; Li, C.; Fan, G.; Li, M.; Huang, H. Recovery of Vanadium from H_2SO_4-HF Acidic Leaching Solution of Black Shale by Solvent Extraction and Precipitation. *Metals* **2016**, *6*, 63. [CrossRef]
4. Wang, M.; Huang, S.; Chen, B.; Wang, X. A review of processing technologies for vanadium extraction from stone coal. *Miner. Process. Extr. Met.* **2018**, *129*, 290–298. [CrossRef]
5. Zhang, B.; Gao, Z.; Liu, H.; Wang, W.; Cao, Y. Direct Acid Leaching of Vanadium from Stone Coal. *High Temp. Mater. Process.* **2016**, *36*, 877–883. [CrossRef]
6. Nayl, A.; Aly, H. Solvent extraction of V(V) and Cr(III) from acidic leach liquors of ilmenite using Aliquat 336. *Trans. Nonferrous Met. Soc. China* **2015**, *25*, 4183–4191. [CrossRef]
7. Suručić, L.T.; Nastasović, A.B.; Onjia, A.E.; Janjić, G.V.; Rakić, A.A. Design of an amino-functionalized chelating macroporous copolymer poly(GMA-co-EGDMA) for the sorption of Cu(II) ions. *J. Serb. Chem. Soc.* **2019**, *84*, 1391–1404. [CrossRef]
8. Suručić, L.T.; Janjić, G.; Rakić, A.A.; Nastasovic, A.; Popović, A.R.; Milčić, M.K.; Onjia, A.E. Theoretical modeling of sorption of metal ions on amino-functionalized macroporous copolymer in aqueous solution. *J. Mol. Model.* **2019**, *25*, 177. [CrossRef]
9. Grochowicz, M.; Pączkowski, P.; Gawdzik, B. Investigation of the thermal properties of glycidyl methacrylate–ethylene glycol dimethacrylate copolymeric microspheres modified by Diels–Alder reaction. *J. Therm. Anal. Calorim.* **2017**, *133*, 499–508. [CrossRef]

10. Nastasovic, A.; Onjia, A.; Milonjic, S.; Jovanović, S. Surface characterization of macroporous glycidyl methacrylate based copolymers by inverse gas chromatography. *Eur. Polym. J.* **2005**, *41*, 1234–1242. [CrossRef]
11. Gupta, S.; Ranjit, R.; Mitra, C.; Raychaudhuri, P.; Pinto, R. Enhanced room-temperature magnetoresistance in $La_{0.7}Sr_{0.3}MnO_3$-glass composites. *Appl. Phys. Lett.* **2001**, *78*, 362–364. [CrossRef]
12. Kango, S.; Kalia, S.; Celli, A.; Njuguna, J.; Habibi, Y.; Kumar, R. Surface modification of inorganic nanoparticles for development of organic–inorganic nanocomposites—A review. *Prog. Polym. Sci.* **2013**, *38*, 1232–1261. [CrossRef]
13. Marković, B.M.; Spasojević, V.V.; Dapcevic, A.; Vuković, Z.M.; Pavlović, V.B.; Ranđelović, D.V.; Nastasović, A.B. Characterization of glycidyl methacrylate based magnetic nanocomposites. *Chem. Ind.* **2019**, *73*, 25–35. [CrossRef]
14. Castro, L.; Ayala, L.A.; Vardanyan, A.; Zhang, R.; Muñoz, J.Á. Arsenate and Arsenite Sorption Using Biogenic Iron Compounds: Treatment of Real Polluted Waters in Batch and Continuous Systems. *Metals* **2021**, *11*, 1608. [CrossRef]
15. Araújo, C.S.; Almeida, I.L.; Rezende, H.C.; Marcionilio, S.M.; Leon, J.J.L.; de Matos, T.N. Elucidation of mechanism involved in adsorption of Pb(II) onto lobeira fruit (*Solanum lycocarpum*) using Langmuir, Freundlich and Temkin isotherms. *Microchem. J.* **2018**, *137*, 348–354. [CrossRef]
16. Webb, P.A.; Orr, C.; Corporation, M.I. *Analytical Methods in Fine Particle Technology*; Micromeritics Instrument Corporation: Norcross, GA, USA, 1997.
17. Marković, B.M.; Vuković, Z.M.; Spasojevic, V.; Kusigerski, V.; Pavlović, V.; Onjia, A.; Nastasović, A.B. Selective magnetic GMA based potential sorbents for molybdenum and rhenium sorption. *J. Alloys Compd.* **2017**, *705*, 38–50. [CrossRef]
18. Maciejewska, M. Thermal properties of TRIM–GMA copolymers with pendant amine groups. *J. Therm. Anal. Calorim.* **2016**, *126*, 1777–1785. [CrossRef]
19. Cascaval, C.; Poinescu, I. Thermal characterization of some cross-linked methacrylic adsorbents. *Polym. Degrad. Stab.* **1995**, *48*, 55–60. [CrossRef]
20. Paredes, B.; González, S.; Rendueles, M.; Villa-García, M.A.; Díaz, M. Influence of the amination conditions on the textural properties and chromatographic behaviour of amino-functionalized glycidyl methacrylate-based particulate supports. *Acta Mater.* **2003**, *51*, 6189–6198. [CrossRef]
21. Qiao, B.; Wang, T.-J.; Gao, H.; Jin, Y. High density silanization of nano-silica particles using γ-aminopropyltriethoxysilane (APTES). *Appl. Surf. Sci.* **2015**, *351*, 646–654. [CrossRef]
22. Dugas, V.; Chevalier, Y. Surface hydroxylation and silane grafting on fumed and thermal silica. *J. Colloid Interface Sci.* **2003**, *264*, 354–361. [CrossRef]
23. Huang, J.-H.; Huang, F.; Evans, L.; Glasauer, S. Vanadium: Global (bio)geochemistry. *Chem. Geol.* **2015**, *417*, 68–89. [CrossRef]
24. Agashe, K.B.; Regalbuto, J.R. A Revised Physical Theory for Adsorption of Metal Complexes at Oxide Surfaces. *J. Colloid Interface Sci.* **1997**, *185*, 174–189. [CrossRef] [PubMed]
25. Perrin, D.D. *Ionisation Constants of Inorganic Acids and Bases in Aqueous Solution*; Pergamon Press Ltd.: Oxford, UK, 1982.
26. Zhang, L.; Liu, X.; Xia, W.; Zhang, W. Preparation and characterization of chitosan-zirconium(IV) composite for adsorption of vanadium(V). *Int. J. Biol. Macromol.* **2013**, *64*, 155–161. [CrossRef] [PubMed]
27. Pennesi, C.; Totti, C.; Beolchini, F. Removal of Vanadium(III) and Molybdenum(V) from Wastewater Using *Posidonia oceanica* (Tracheophyta) Biomass. *PLoS ONE* **2013**, *8*, e76870. [CrossRef] [PubMed]
28. Ekmeščić, B.M.; Maksin, D.D.; Markovic, J.P.; Vuković, Z.M.; Hercigonja, R.V.; Nastasović, A.B.; Onjia, A.E. Recovery of molybdenum oxyanions using macroporous copolymer grafted with diethylenetriamine. *Arab. J. Chem.* **2019**, *12*, 3628–3638. [CrossRef]
29. Marjanovic, V.; Peric-Grujic, A.; Ristic, M.; Marinkovic, A.; Markovic, R.; Onjia, A.; Sljivic-Ivanovic, M. Selenate Adsorption from Water Using the Hydrous Iron Oxide-Impregnated Hybrid Polymer. *Metals* **2020**, *10*, 1630. [CrossRef]
30. Hercigonja, R.V.; Maksin, D.D.; Nastasović, A.B.; Trifunović, S.S.; Glodić, P.B.; Onjia, A.E. Adsorptive removal of technetium-99 using macroporous poly(GMA-co-EGDMA) modified with diethylene triamine. *J. Appl. Polym. Sci.* **2011**, *123*, 1273–1282. [CrossRef]
31. Weidner, E.; Ciesielczyk, F. Removal of Hazardous Oxyanions from the Environment Using Metal-Oxide-Based Materials. *Materials* **2019**, *12*, 927. [CrossRef]
32. Foo, K.Y.; Hameed, B.H. Insights into the modeling of adsorption isotherm systems. *Chem. Eng. J.* **2010**, *156*, 2–10. [CrossRef]
33. Dongil, A.B.; Bachiller-Baeza, B.; Guerrero-Ruiz, A.; Rodríguez-Ramos, I.; Martínez-Alonso, A.; Tascón, J.M.D. Surface chemical modifications induced on high surface area graphite and carbon nanofibers using different oxidation and functionalization treatments. *J. Colloid Interface Sci.* **2011**, *355*, 179–189. [CrossRef] [PubMed]